Biosensors and Bioelectronics 102 (2018) 668–675

Contents lists available at ScienceDirect

Biosensors and Bioelectronics

journal homepage: www.elsevier.com/locate/bios

Multi-parametric rigid and flexible, low-cost, disposable sensing platforms for biomedical applications

Salzitsa Anastasova[1], Panagiotis Kassanos[1], Guang-Zhong Yang*

The Hamlyn Centre, Imperial College, London, UK

ARTICLE INFO

Keywords:
PCB electrode
Ion sensors
Flexible
Multi-parametric
Potentiometric sensors

ABSTRACT

The measurement of Na^+, K^+ and H^+ is essential in medicine and plays an important role in the assessment of tissue ischemia. Microfabrication, inkjet- and screen-printing can be used for solid contact ion selective electrodes (ISE) realization; these, however, can be non-standardized, costly and time consuming processes. We present the realization of ISEs on post-processed electrodes fabricated via standardized printed circuit board (PCB) manufacturing techniques. *In vitro* results are presented from two rigid platforms (32 ISEs) for liquid sample dip-stick measurements and two flexible platforms (6 and 32 ISEs) for post-surgical intestinal tissue monitoring, each with a common reference electrode (RE). These are combined with optimized tetrapolar bioimpedance sensors for tissue ischemia detection. Both electroless and hard gold PCB finishes are examined. Apart from the electroless rigid platform, the rest demonstrated comparable and superior performance, with the pH sensors demonstrating the greatest deviation; the flexible hard gold platform achieved a sensitivity 4.6 mV/pH and 49.2 mV/pH greater than the electroless flexible and rigid platforms, respectively. The best overall performance was achieved with the hard gold flexible platform with sensitivities as large as 73.4 mV/pH, 56.3 mV/log [Na^+], and 57.4 mV/log [K^+] vs. custom REs on the same substrate. Simultaneous measurement of target analytes is demonstrated with test solutions and saliva samples. The results demonstrate superior performance to other PCB-based pH sensors and Na^+ and K^+ PCB-based sensors with comparable performance to potentiometric sensors fabricated with other techniques, paving the way towards mass-produced, low-cost, disposable, multi-parametric chemical sensing diagnostic platforms.

1. Introduction

The measurement of various ionic species is essential in biomedical applications where, for example, sensor-enabled surgical drains, catheters and implants with high accuracy, minimal drift, low cost and disposability are needed. Electrolyte homeostasis is vital for human health, as many metabolic processes and organ functions depend on it. Consequently, its disturbance can be detrimental and it is associated with increased morbidity, mortality and prolonged overall hospital stay. Tissue ischemia (i.e. insufficient tissue oxygenation) disturbs homeostasis and leads to changes in tissue pH, while the intracellular and extracellular concentrations of K^+ and Na^+ also change due to failure of the cell membrane pumps (Chung et al., 2014; Cosofret et al., 1995; Mir et al., 2014; Tahirbegi et al., 2013, 2014). Monitoring these ions can thus provide valuable insights into the state of tissues. In surgical intestinal anastomosis, one of the most challenging complications is anastomotic leakage (AL) (Millan et al., 2006; Nerstrom et al., 2016). Tissue oxygenation is essential for the healing of an anastomosis and thus plays a dominant role in AL. Currently, ALs are diagnosed at a mean time of 12 days post-operatively (Chadi et al., 2016). Within 24 h post-operation, intramucosal pH of less than 7.28 has been reported in patients who went on to develop AL (Hirst et al., 2014; Millan et al., 2006).

Microfabrication techniques are used to pattern metal electrodes and deposit selective membranes onto rigid, flexible and stretchable substrates (Chung et al., 2014). However, these approaches can be costly since often these are not standardized processes readily available for mass production. Alternative techniques include screen-printing (Fay et al., 2011) and inkjet-printing (Komuro et al., 2013; Sjoberg et al., 2016). The latter is a maskless fabrication method with reduced ink waste. It is, however, mainly limited to research laboratories. The optimization of the printing parameters is a laborious process and, being a direct-write technique, it is not suitable for high-throughput batch-fabrication.

The realization of electrodes fabricated using standard, widely available commercial printed circuit board (PCB) technologies presents a simple, low-cost solution for the production of different sensors,

* Corresponding author.
E-mail addresses: s.anastasova-ivanova@imperial.ac.uk (S. Anastasova), p.kassanos@imperial.ac.uk (P. Kassanos), g.z.yang@imperial.ac.uk (G.-Z. Yang).
[1] S.A. and P.K. contributed equally to this work.

http://dx.doi.org/10.1016/j.bios.2017.10.038
Received 21 July 2017; Received in revised form 15 October 2017; Accepted 16 October 2017
Available online 18 October 2017

where the potential for large-volume production allows economies of scale to significantly reduce the cost. In (Bozkurt and Lal, 2011) an implantable flexible PCB microelectrode array was presented for extracellular stimulation in invertebrates. The Cu structures were Au-plated either chemically (electroless or immersion plating) or electrochemically (electroplating). The latter resulted in greater surface roughness (hence a larger electroactive surface) and complete electrode Au-coating, as opposed to the former, where electrode side walls were left uncoated. To address this, the top passivation opening was made smaller than the electrode, such that the electrode sidewalls are not exposed. In (Kassanos et al., 2015), a flexible PCB-based tetrapolar bioimpedance sensor was presented with optimized geometry and electric field properties for monitoring the mucosa of the intestinal tract during induced ischemia in a porcine model.

The use of PCB electrodes for the realization of potentiometric sensors was examined in the work of (Moschou et al., 2015; Prodromakis et al., 2011; Trantidou et al., 2013). In (Prodromakis et al., 2011) Au-plated Cu electrodes (500 μm in diameter) on rigid PCB substrates were coated by sputtering 150 nm TiO_2. This lead to a sensitivity to H^+ of ~ −22 mV/pH. The same PCB electrode structure was used in (Trantidou et al., 2013) where a Parylene C film deposited on the PCB was selectively plasma-treated, leading to a sensitivity of −16.3 mV/pH and drift rates of 2.5–20 mV/h. In (Moschou et al., 2015) rigid-PCB-based Ag/AgCl reference electrodes (RE) based on vias with diameters of 300 μm to 1 mm were presented. These achieved a drift less than 1 mV/20 days at pH 7. Together with a PCB-based pH sensor utilizing a 200 nm thick indium tin oxide (ITO) layer, a sensitivity of −45.8 mV/pH was demonstrated.

In this paper, the realization of ISEs on post-processed electrodes fabricated using standardized PCB manufacturing is presented. Results are presented from two rigid 34-electrode arrays intended as dip stick measurement platforms for liquid sample analysis (e.g. urine, blood, saliva), each using different Au-plating. The work was then extended to two flexible PCBs. One is intended to be wrapped as a ring to be placed within the intestinal lumen to monitor tissue ischemia following surgical anastomosis. The second platform is a miniaturized patch for the same application. To the author's knowledge, this is the first example of such multi-parametric sensing systems with rigid or flexible PCB technologies. This paper presents a number of novelties: (i) demonstration of K^+ and Na^+ PCB-based potentiometric sensors, (ii) PCB-based pH sensors with improved performance, (iii) examination of both electroless and electrochemical PCB Au-plating on sensing performance, (iv) incorporation of custom REs on the same substrate with the ISEs forming multi-electrode multi-parametric potentiometric sensing arrays, (v) use of commercially fabricated flexible PCBs and (vi) incorporation on the substrate of an optimized tetrapolar bioimpedance tissue ischemia sensor (Kassanos et al., 2015), allowing multi-modal sensing.

2. Materials and methods

2.1. Design and fabrication of PCBs

All electrode arrays were designed using Altium Designer version 15.1.16 (Altium, Ltd.). Commercial PCB manufacturers (Eurocircuits, Mechelen, Belgium and P.W. Circuits, Leicester, UK) were used for the fabrication of the electrode platforms of Fig. 1. Rigid FR-4 (flame retardant), flexible polyimide (PI) substrates, liquid photoimageable solder masks (LPSM), PI coverlays, electroless nickel immersion gold (ENIG) and hard gold finishes were used for the various designs, as summarized in Table 1. A discussion on materials used in PCB manufacturing can be found in the Supplementary information (SI, Section S1, Table S1, S2).

2.2. Electrode post-processing and functionalization

All experiments are performed using an Ivium potentiostat/galvanostat (Ivium Technologies, Netherlands). Cyclic voltammetry, including electrochemical electrode cleaning (using a solution of 50 mM H_2SO_4 and a sweep potential between −0.4 and 0.6 V at 100 mV/s) and electropolymerisation, were performed in three-electrode mode using a commercial Ag/AgCl BASI RE and a Pt counter electrode in a N_2 purged solution. Double-distilled (DI) water was used for the preparation of all solutions. Further details on electrode post-processing and functionalization can be found in the SI (Section S2).

Microscope images were obtained with a Keyence VHX-2000 microscope. Atomic force microscopy (AFM) images where obtained with an Asylum Research (Ca, USA) MFP-3D Classic AFM instrument. Images of 10 μm × 10 μm electrode areas where acquired using the tapping mode and PPP-NCHR probes. The obtained AFM images were analysed using the WSxM1 software (Horcas et al., 2007).

3. Results

3.1. Rigid and flexible electrode platform designs

The four platforms developed are summarized in Table 1. The electrodes of Fig. 1(a), (b) and (c) were of 1 mm diameter, however, the exposed area of the electrode was defined by a 500 μm diameter solder mask opening similar to (Bozkurt and Lal, 2011), to avoid the exposure of partially plated Cu or Ni from the edges and sidewalls of the electrodes. Platforms 1 and 2 were laid out to form a ~ 10 cm long dip stick and are simply the rigid equivalents of Platform 3 (Fig. 1(c)). The minimum track width and distance between tracks was 150 μm, and 45° angles were used in the interconnects (Fig. 1(a)(i), (b)(i) and (c)(i)).

Platform 3 is intended to be wrapped in a ring to be placed within the intestinal tract lumen in the vicinity of an anastomosis in order to monitor tissue ischemia as an early marker for anastomotic leakage (Hirst et al., 2014; Kassanos et al., 2015), as illustrated in Fig. S1(a), (b). This was designed such that it fits a large array of electrodes within a 2.5 cm diameter suitable to fit within the small intestine and to allow mapping of the target analytes along the anastomosis. The electronics based on a 32:1 multiplexer (Analog Devices ADG732) also constrained the electrode number. The additional 2 electrodes are used as a common reference electrode and as a biasing electrode for differential measurements (similar to (Hammond et al., 2004)).

Platform 4 is a small flexible patch (Fig. 1(d)) for small tissue area assessment, with 100 μm minimum track width and distance between tracks. As evident from the CAD (computer aided design) layout of Fig. 1(d)(ii), rounded corners and teardrop connections to the bonding pads located on the bottom side of the board were also used. These allow greater flexibility and durability of the tracks. The electrodes are 400 μm in diameter and the active region of the electrode is defined by a 300 μm opening in the coverlay. There are 6 electrodes for the development two pH, Na^+ and K^+ sensors, one extra bias electrode and a large parallelogram electrode (400 μm × 1.35 mm copper structure with a coverlay opening defining the RE area of 300 μm × 1.3 mm) to serve as a common RE. This device is intended as a miniature multi-parametric sensing patch that can be interrogated by a dedicated application specific integrated circuit (ASIC), which is currently being designed, as in Fig. S1(c).

In all platforms, a tetrapolar bio-impedance sensor (Kassanos et al., 2015) optimized for tissue ischemia monitoring in the gastrointestinal tract is also incorporated. In Platform 3 the additional bio-impedance sensor is based on the design of (Ivorra et al., 2003). The combination of ionic measurements with electrical bioimpedance allows their corroboration, as tissue impedance changes are related to ischemia.

In all platforms, more than one electrode is allocated for each analyte. In Platform 3, this allows assessing ionic concentrations over large tissue areas. In all platforms, it also provides averaging and redundancy, i.e. having additional sensors if one fails and a way to minimize false positives/negatives.

It is evident from the images of Fig. 1(a), (b) and (c), that the electrode surface is rough and that there are scratch-marks on the

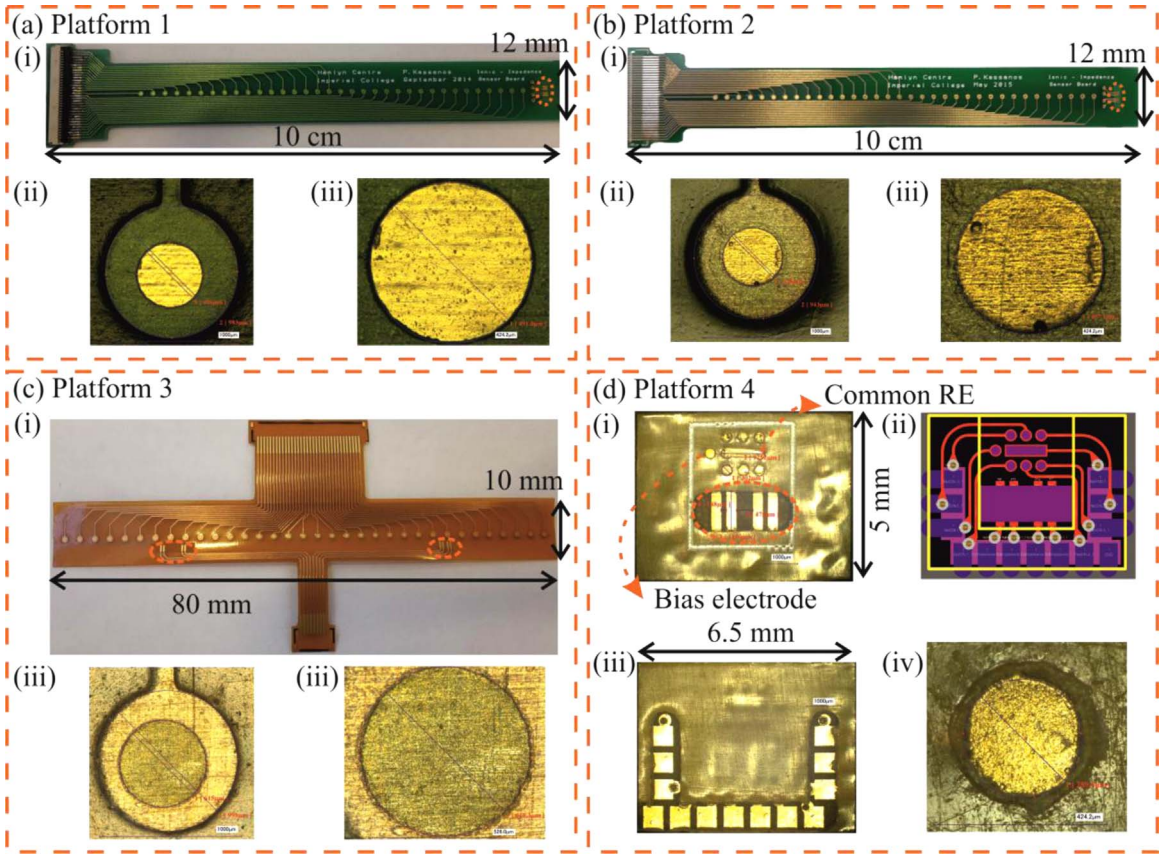

Fig. 1. Platform 1: Rigid with ENIG finish. Platform 2: Rigid with hard gold finish. Platform 3: Flexible ring array with ENIG finish. Platform 4: Two-layer flexible patch with hard gold finish. In (a)(i), (b)(i), (d)(i) and on the right of (c)(i) within the dotted orange markers is the tetrapolar impedance sensor of (Kassanos et al., 2015). The sensor within the dotted orange marker on the left of (c)(i) is the structure of (Ivorra et al., 2003). (For interpretation of the references to color in this figure legend, the reader is referred to the web version of this article.)

electrode surface from the fabrication process, PCB testing, handling and packaging; surface roughness and Au-film pinholes expose the underlying Cu or Ni. These hinder the electrochemical properties of the electrodes and the quality of the subsequently deposited layers for ISE realization. This is also evident in the AFM images of Fig. 2(a)(ii)-(iii) obtained with Platform 2. From the AFM images of Fig. 2(b), it is clear that the additional Au nanoparticle electrodeposition (see SI Section S2) results in a homogeneous and smoother surface structure compared with the initial electroplated Au film. The additional layer of Au is approximately 20 nm thick. The surface topography of an electrode following deposition of the IrOx pH sensing membrane after Au nanoparticle deposition is shown in Fig. 2(c). The thickness of the final film is equal to 80.6 nm. As demonstrated in the figures, the surface inhomogeneity and defects of the area are further reduced.

3.2. Potentiometric sensor characterization

Sample graphs demonstrating the performance of the sensors from various platforms are shown in Figs. 3 and 4. Table 2 summarizes in detail the analytical performance of the sensors developed with all four platforms. The performance of the RE is crucial for all electrochemical sensing systems. In potentiometric sensor arrays, a single RE can be used. REs were developed and tested on all four platforms, demonstrating similar performance. Their only difference was the offset voltage with respect to the conventional RE used for initial validation. The well-established methods of (Mattinen et al., 2009) were used for the study of the stability of the developed PCB-based solid-contact RE. The results of Fig. 3(a) were obtained with the RE developed using Platform 2 and are compared with the response of a conventional RE. Changes of the mobility of the electrolyte and concentration differences using 0.1 M KCl, 10^{-4} M KCl, 10^{-4} M NaCl, 0.1 M NaCl and 0.1 M KCl are shown, demonstrating the stability of the RE. All subsequent results from the pH, Na^+ and K^+ sensors are obtained using the corresponding custom REs of each platform and not commercial REs.

In order to demonstrate the effect of the electrode pre-treatment steps on the performance of the sensors, Platform 1 is compared with and without any pre-treatment, including the electrodeposited additional layers of Au nanoparticles and PEDOT (see SI Section S2 and Fig. 2). For example, untreated Platform 1 electrodes achieved measurements for sodium in the range between 10^{-4} M to 10^{-1} M with a

Table 1
Description of the platforms of Fig. 1.

	Substrate	Finish	Top Insulation	Number of Electrodes	Electrode Active Area	Vendor
Platform 1	1.55 mm FR-4 18 μm Cu (Rigid)	ENIG	LPSM	34	500 μm	Eurocircuits
Platform 2	1.55 mm FR-4 18 μm Cu (Rigid)	Hard Au	LPSM	34	500 μm	P.W. Circuits
Platform 3	250 μm PI 35 μm Cu (Flexible)	ENIG	LPSM	34	500 μm	P.W. Circuits
Platform 4	250 μm PI 18 μm Cu (Flexible)	Hard Au	250 μm PI Coverlay	8	300 μm and RE: 300 μm × 1.3 mm	P.W. Circuits

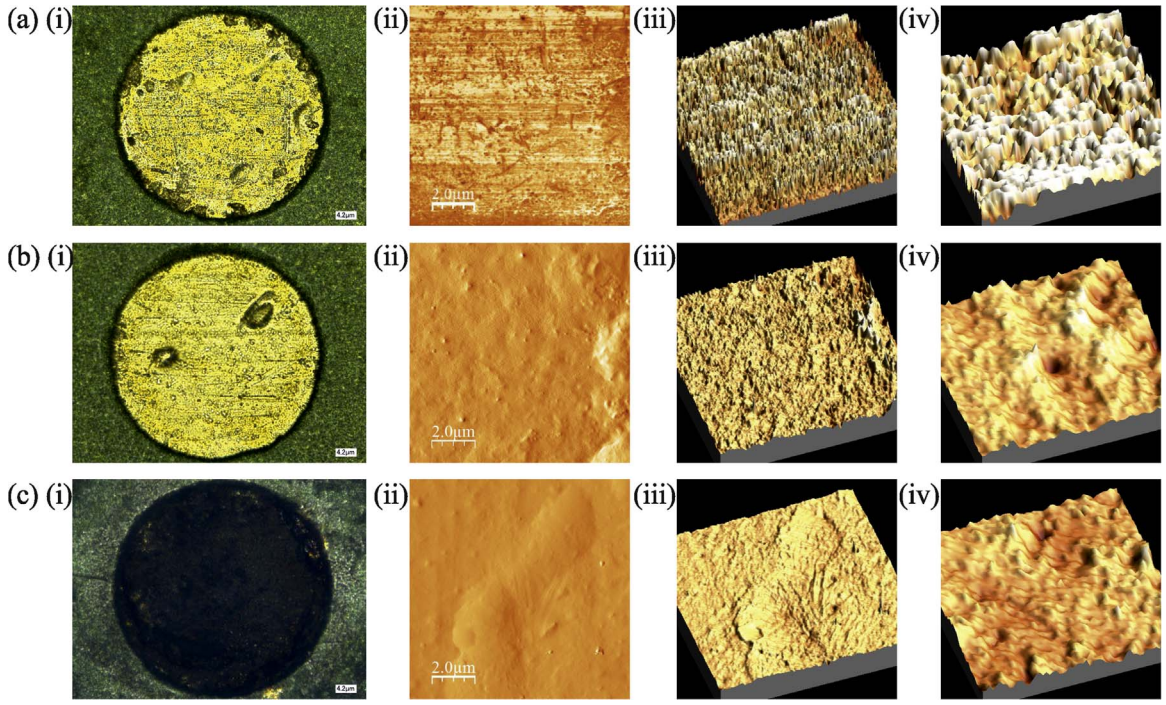

Fig. 2. Imaging of Platform 2. (a) Unmodified electrode: (i) microscope image, (ii) AFM 2D image, (iii) AFM 3D image. (b) Electrode with additional electrodeposited layer of 10 nm Au nanoparticles: (i) microscope image, (ii) AFM 2D image, (iii) AFM 3D image. (c) Electrodeposited pH sensing IrOx membrane: (i) microscope image, (ii) AFM 2D image, (iii) AFM 3D image.

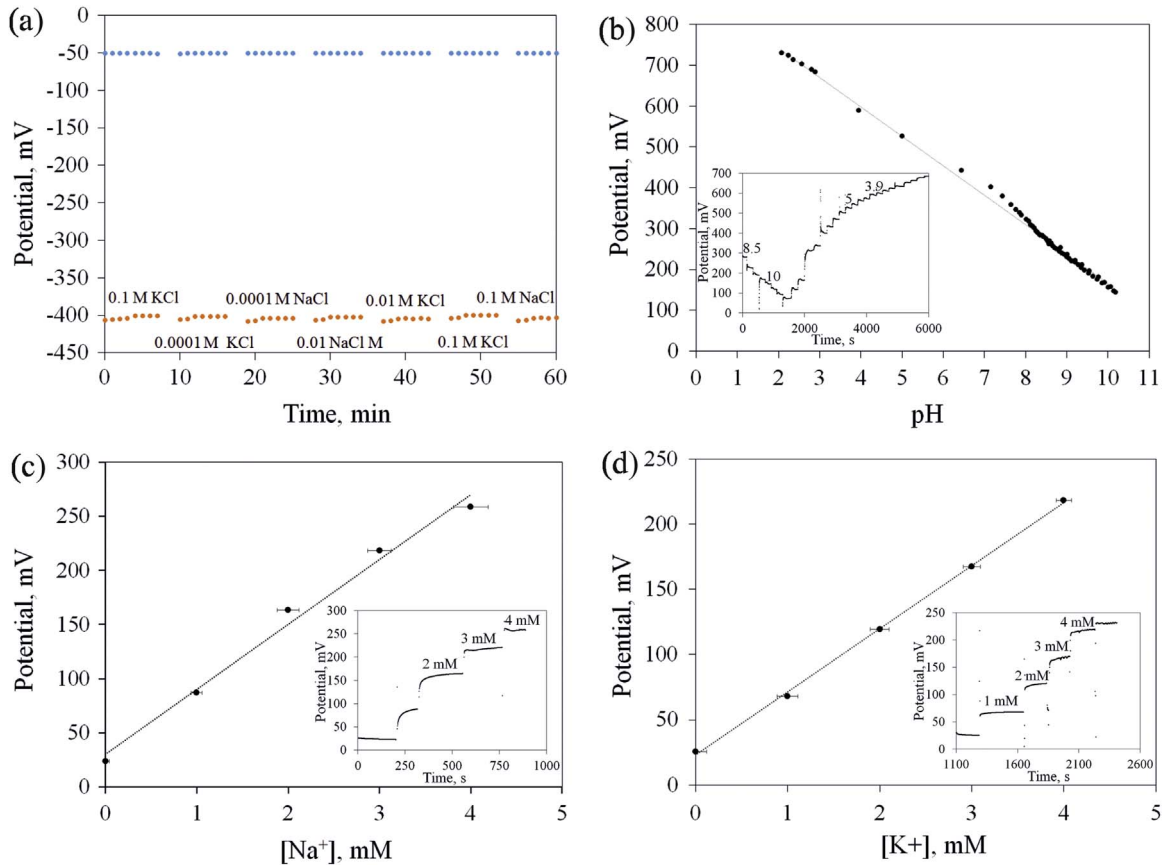

Fig. 3. (a) Potential response (to salt solutions) of conventional RE (blue dots) and solid-contact RE (orange dots) developed on Platform 2 (Fig. 1b). Calibration curves and transient responses of the (b) pH, (c) sodium and (d) potassium sensors developed using Platform 2. (For interpretation of the references to color in this figure legend, the reader is referred to the web version of this article.)

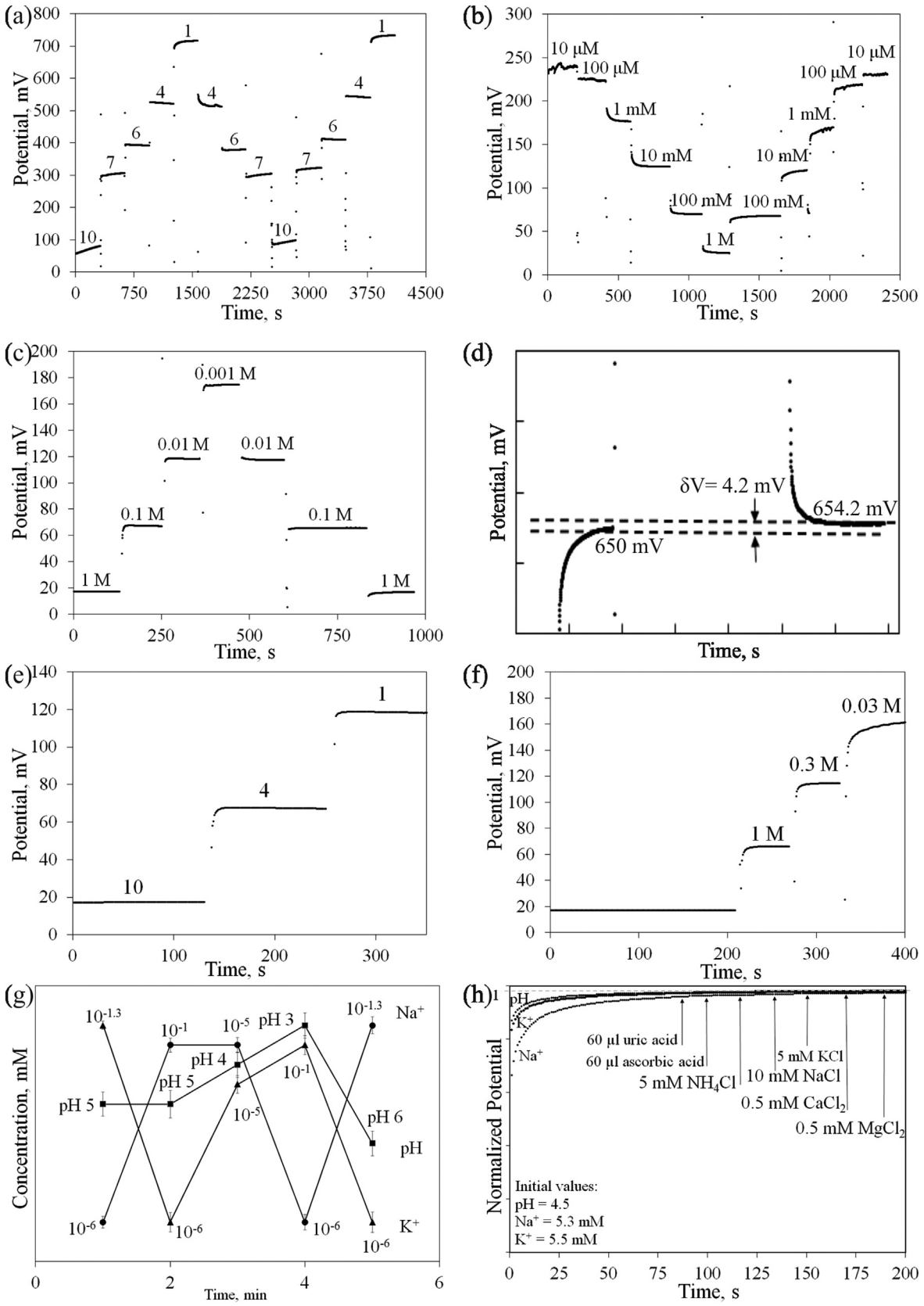

Fig. 4. Carry-over testing for (a) pH between 10 to 1; (b) [Na^+] in the range between 10^{-5} to 1 M; (c) [K^+] in the range between 10^{-5} to 1 M; (d) hysteresis (*dV*) as a factor for reversibility. There results were obtained using the IrOx pH sensor developed with Platform 4 (Fig. 1(d)). Changes of (e) pH and (f) sodium using Platform 4. The sensors demonstrate fast response time to concentration changes (see Table 2). (g) Simultaneous measurement of all three target analytes with Platform 2 at different concentrations. (h) Normalised potentiometric responses upon the addition of interfering species.

Table 2
Average sensitivity and intercept values, response time, LOD and drift obtained from all four platforms, one of which (Platform 1) is compared with and without the relevant pre-treatment steps (see SI section S2).

Na^+ selective electrode							
Platform	**Sensitivity (mV/log [Na^+])**	**%RSD**	**Intercept (mV)**	**%RSD**	**Response time (s)**	**LOD (M)**	**Drift mV/24 h**
Platform 1 untreated	12.2 ± 3.5	3.5	178.9 ± 5.6	3.2	420	10^{-3}	50
Platform 1*	22.2 ± 1.9	4.5	186.1 ± 3.5	3.7	300	10^{-4}	28.9
Platform 2 *	54 ± 1.5	2.5	241.5 ± 2.3	1.2	200	10^{-4}	23.2
Platform 3 *	55.8 ± 1.2	3.2	251.3 ± 3.2	1.3	150	10^{-4}	17.6
Platform 4 *	56.3 ± 0.9	2.5	250 ± 4.2	0.6	30	10^{-5}	16.5
K^+ selective electrode							
Platform	**Sensitivity (mV/log [K^+])**	**%RSD**	**Intercept (mV)**	**%RSD**	**Response time (s)**	**LOD (M)**	**Drift mV/24 h**
Platform 1 untreated	12.2 ± 7.5	6.2	178.9 ± 5.6	4.5	460	10^{-3}	59.9
Platform 1 *	22.2 ± 4.9	5.4	186 ± 3.5	4.1	300	10^{-4}	28.6
Platform 2 *	54 ± 2.5	3.5	241.5 ± 2.3	1.9	250	10^{-4}	32.4
Platform 3 *	55.8 ± 1.2	2.4	249.3 ± 2.4	2.5	180	10^{-4}	24.8
Platform 4 *	57.4 ± 1.9	1.9	250 ± 4.2	2.9	40	10^{-5}	19.6
pH selective electrode							
Platform	**Sensitivity (mV/log [H^+])**	**%RSD**	**Intercept (mV)**	**%RSD**	**Response time (s)**	**LOD**	**Drift mV/24 h**
Platform 1 untreated	−24.2 ± 2.5	3.1	150.5 ± 5.6	3.4	300	6 units	52
Platform 1 **	−25.6 ± 1.6	3.5	161.3 ± 3.5	2.8	150	3.5 units	26.5
Platform 2 **	−59 ± 1.8	2.2	116.9 ± 2.3	1.1	50	2.6 units	20
Platform 3 **	−69.8 ± 0.8	3	116 ± 2.8	1.2	30	3.5 units	10
Platform 4 **	−73.4 ± 0.6	2.6	118 ± 4.2	0.9	10	2.4 units	4.2

* + Au nanoparticles and PEDOT.
** + Au nanoparticles.

slope of 12.2 mV/log [Na+] and an intercept at 178.9 mV, while when pre-treated the slope is 22.2 mV/log [Na+] with an intercept of 186.1 mV. Fig. 3(b), (c) and (d) show the transient response and the calibration curves of each sensor developed using Platform 2. As summarized in Table 2, sensitivities of -59 mV/pH for pH, 54 mV/log [Na^+] for Na^+ and 54 mV/log [K^+] for K^+ were achieved. When these sensors were kept in dry conditions, an initial decrease of 10% of sensitivity was observed. Soaking these electrodes for 1 h in buffer solution restored their sensitivity to the original value (Ges et al., 2005).

To examine their repeatability, sensors were cycled between different concentrations of target analytes. Fig. 4(a)-(d) demonstrates the results for sensors developed using Platform 4. It is evident from the figure that the repeatability of all sensors is very good over time. The IrOx pH sensor achieved a super-Nernstian sensitivity of -73.4 mV/pH with a limit of detection (LOD) of 2.4 pH units. On the other hand the Na^+ sensor demonstrated a sensitivity of 56.3 mV/log [Na^+], within a linear working range from 10^{-4} M up to 10^{-1} M and a LOD of 10^{-5} M. The K^+ sensor also demonstrated a Nernstian response of 57.4 mV/log [K^+] from 10^{-4} M up to 10^{-1} M and a LOD of 10^{-5} M.

The hysteresis of the pH sensors (Platform 4) was assessed and is shown in Fig. 4(d). The observed deviation could be related to the electronic noise or interferences and motion artifacts, such as liquid motion and temperature changes (as the test solutions were not thermally stabilized during the experiments), and is defined as the difference in measured potential (δV) between different tests when using the same electrode in the same solution. The potential stabilization is obtained in 10 s and the observed δV is 4.2 mV during the first two additions of pH 2.4 and 3, which is significantly smaller than that reported elsewhere, e.g. δV = 23.7 mV in (Huang et al., 2011) for pH 1.5. The observed hysteresis in our platform for pH 3 onwards was much smaller than 0.3 mV reported from (Huang et al., 2011) for pH 3.75. The obtained hysteresis is minimized by optimization of the thickness, amorphousness and porosity of the membrane through controlled electrodeposition. In the case of the flexible PCB with ENIG finish (Platform 3) a hysteresis of 1 mV, 17.6 mV and 24.8 mV were observed which were constant throughout the working range of the pH, sodium and potassium sensors, respectively.

The response and settling times of the sensors were also examined in detail and are summarized in Table 2. It is quite obvious that, in addition to improving sensor sensitivity, electrode pre-treatment (see SI section S2) minimizes sensor drift. The observed drift of the IrOx pH sensors realized with Platform 1 is reduced to 26.5 mV/24 h from 52 mV/24 h with the additional pre-treatment (Table 2). As an example, Fig. 4(e)-(f) show the results from the sensors with high sensitivity and fast response obtained with Platform 4, where the signal reaches steady-state within 10 s for the pH sensor and 30 s for the sodium sensor. It can be seen that, once in steady state, the sensor's output signal remains stable. The response time without pre-treatment, according to the data of Table 2, is very slow. It is found to be 5 min for the pH sensor and 7 min for the sodium sensor, and the deviations are significant.

The best overall results were obtained with Platform 4. The above described platforms are compared with other potentiometric PCB-based platforms in Table S3, and with other ISEs and REs developed using established fabrication techniques in Tables S4, S5, S6 and S7 in the SI.

Tissue ischemia induces changes to the concentrations of pH, Na^+ and K^+, which are interrelated and thus provide a means of corroborating measurements. Consequently, simultaneous measurement of all three analytes for Na^+ and K^+ concentrations between 10^{-6} and 10^{-1} mM and pH 3–6 using Platform 2 was assessed and is shown in Fig. 4(g). Selectivity is important to differentiate and monitor these with high specificity and in the presence of other interfering analytes. To evaluate this, the effect of varying amounts of different interfering analytes, (e.g. 60 µl uric acid, 60 µl ascorbic acid, 10 mM NaCl, 5 mM KCl, 5 mM NH_4Cl, 0.5 mM $MgCl_2$ and 0.5 mM $CaCl_2$), on the sensors was examined using Platform 2. This is shown in Fig. 4(h). This was repeated in a saliva sample obtained from a healthy 35 year old subject (Fig. S2). To demonstrate the applicability of the proposed sensors in

real samples, multipoint real-time measurements of saliva samples were performed to assess Na^+ and K^+ ion content as a function of exercise, which is related to ischemia. These are shown in Fig. S3. Further details are included in the SI (Section S3).

4. Discussions

Pre-treatment of electrode structures with Au nanoparticles, before deposition of the ion sensitive membranes, is crucial for the behaviour and response of the sensors (Fig. 2). Without pre-treatment of Platform 1, significantly smaller sensitivities (e.g. 12.2 mV/log [Na^+] vs. 22.2 mV/log [Na^+]) and slower responses (e.g. 5 min vs. 10 s to reach steady state with the pH sensors) were achieved (Table 2). Electrodeposition of the intermediate layer on the electrodes produced identical response curves, leading to excellent sensor reproducibility. These electrodes were successfully utilised for the determination of Na^+, K^+ and pH in the samples.

The stability of the RE was evaluated through measurements in salt solutions with different concentrations (Fig. 3(a)). In the ideal case, we have minimal/no change in signal regardless of the sample composition. The initial slow response is related to the kinetic hindrance due to surface ion-exchange processes (Mattinen et al., 2009). Compared with (Moschou et al., 2015), where the reported RE demonstrated a drift of 1 mV/20 days, our REs demonstrated no more than 0.03 mV deviations during 60 min tests, allowing the development of reliable, stable, compact multi-parametric platforms of high sensitivity sensors in a single PCB.

Long-term stability and reproducibility was excellent. Our studies showed good stability and repeatability of over 8 months for the pH sensor, over 6 weeks for the Na^+ sensor and over 4 weeks for the K^+ sensor. Good reproducibility, stability, and repeatability while using pre-processed platforms and changing the sodium, potassium, pH concentrations within the physiological range, demonstrated the ability of the platforms to accommodate potentiometric detection of several ions (Figs. 3 and 4). As it can be seen from Fig. 4(h), the proposed sensors demonstrated excellent selectivity in the presence of the examined interfering analytes; no observable influence on the measurements was recorded. This is further supported by the interference experiments performed with a saliva sample (Fig. S2 in SI). The observed initial changes in the range of 10–15 mV during each added analyte is a result of initial 10 s equilibrium of the sensors.

Sensors developed with Platform 3 and Platform 4 achieved similar performance, with sensors developed with Platform 4 performing marginally better (Table 2). We believe this is due to the hard Au finish being an electrode material that is better suited to electrochemical sensors, because the former has a larger electroactive surface as reported in (Bozkurt and Lal, 2011). Nevertheless, the small difference in performance means that the cheaper ENIG finish can be used, without much of a performance trade-off (Table 2). On the other hand, the difference between the ENIG and hard Au finish on the rigid platforms (Platform 1 and 2, respectively) was substantial. Platform 1 was fabricated by a different manufacturer from the other 3 platforms. This potentially shows a difference between the quality of the electrodes as a function of the manufacturer and their specific processes. Further work is needed to verify this using PCBs manufactured from a range of different vendors. The lowest LODs were achieved with Platform 4. These were detection of pH equal to 2.4 and sodium and potassium concentrations of 10^{-5} M. Response times of ~ 10 s, 30 s, 40 s for the pH, sodium and potassium sensors respectively, were achieved with this platform. Finally, the results of Fig. 4(g) and S3 demonstrate the ability of the proposed platforms to simultaneously determine the targeted ionic species in controlled and real samples.

The proposed pH sensors demonstrate improved performance when compared to the state of the art (Table S3), while the current work has explored the realization of potentiometric PCB sensors beyond pH sensors, demonstrating the development of K^+ and Na^+ sensors for the first time. In addition, these have been combined to realize standalone multi-parametric potentiometric sensing platforms with on-PCB REs for the first time. As highlighted in Table S3, being entirely electrodeposited, the IrOx pH sensing membrane is fully compatible with the current PCB fabrication processes. We are currently developing electrodeposition methods for the realization of the K^+, Na^+ and RE membranes such that they can also be compatible with the mass-fabrication processes of the PCB industry. Comparison with ISEs developed with established methods in Tables S4, S5, S6 and S7, demonstrates comparable performance to the proposed work.

5. Conclusions

In this paper multi-parametric potentiometric sensing platforms for biomedical applications were presented based on PCB technology. Such platforms have been achieved through the incorporation of several vital features. A stable RE was developed and was incorporated and tested together with the developed ion sensors on a common substrate to develop platforms that are low-cost, reliable, robust and easy to be implemented or integrated into any future sensing applications. The use of PCB technologies allows the incorporation of both electronics and sensing on the same platform. Post-processing (with additional electrochemical deposition of gold or gold and PEDOT) of the initial, much cheaper ENIG platforms gave similar results as the hard Au finish, which is more expensive and is consequently not essential if a small decrease in performance is tolerated. The favorable comparisons with the state of the art in PCB-based potentiometric sensing and equivalent performance with conventionally-fabricated devices, paves the way towards mass-produced, low-cost, disposable, multi-parametric chemical and multi-modal point of care (POC) diagnostic platforms required both in the developed (for the decentralization of healthcare) and the developing worlds.

Acknowledgments

This work is funded by the UK Engineering and Physical Sciences Research Council (EPSRC) through the Smart Sensing for Surgery Project (EP/L014149/1). The authors would like to thank I. F. Triantis (City University) for early discussions on ISEs and ISFETs, V. Curto (École Nationale Supérieure des Mines de Saint-Étienne) for initial help with IrOx deposition on PCB electrodes, V. Bemmer (Imperial College London) for training and assistance with AFM measurements, F. Seichepine (Hamlyn Centre) and I. Kassanos (National Technical University of Athens) for valuable comments, M. Power (Hamlyn Centre) for her help proof-reading the manuscript.

Appendix A. Supporting information

Supplementary data associated with this article can be found in the online version at http://dx.doi.org/10.1016/j.bios.2017.10.038.

References

Bozkurt, A., Lal, A., 2011. Sens. Actuators a-Phys. 169 (1), 89–97.
Chadi, S.A., Fingerhut, A., Berho, M., DeMeester, S.R., Fleshman, J.W., Hyman, N.H., Margolin, D.A., Martz, J.E., McLemore, E.C., Molena, D., Newman, M.I., Rafferty, J.F., Safar, B., Senagore, A.J., Zmora, O., Wexner, S.D., 2016. J. Gastrointest. Surg. 20 (12), 2035–2051.
Chung, H.J., Sulkin, M.S., Kim, J.S., Goudeseune, C., Chao, H.Y., Song, J.W., Yang, S.Y., Hsu, Y.Y., Ghaffari, R., Efimov, I.R., Rogers, J.A., 2014. Adv. Healthc. Mater. 3 (1), 59–68.
Cosofret, V.V., Erdosy, M., Johnson, T.A., Buck, R.P., Ash, R.B., Neuman, M.R., 1995. Anal. Chem. 67 (10), 1647–1653.
Fay, C., Anastasova, S., Slater, C., Buda, S.T., Shepherd, R., Corcoran, B., O'Connor, N.E., Wallace, G.G., Radu, A., Diamond, D., 2011. IEEE Sens. J. 11 (10), 2374–2382.
Ges, I.A., Ivanov, B.L., Schaffer, D.K., Lima, E.A., Werdich, A.A., Baudenbacher, F.J., 2005. Biosens. Bioelectron. 21 (2), 248–256.
Hammond, P.A., Ali, D., Cumming, D.R.S., 2004. IEEE Sens. J. 4 (6), 706–712.
Hirst, N.A., Tiernan, J.P., Millner, P.A., Jayne, D.G., 2014. Colorectal Dis. 16 (2), 95–109.

Horcas, I., Fernandez, R., Gomez-Rodriguez, J.M., Colchero, J., Gomez-Herrero, J., Baro, A.M., 2007. Rev. Sci. Instrum. 78 (1).
Huang, W.D., Cao, H., Deb, S., Chiao, M., Chiao, J.C., 2011. Sens. Actuators A-Phys. 169 (1), 1–11.
Ivorra, A., Gomez, R., Noguera, N., Villa, R., Sola, A., Palacios, L., Hotter, G., Aguilo, J., 2003. Biosens. Bioelectron. 19 (4), 391–399.
Kassanos, P., Ip, H.M.D., Yang, G.Z., 2015. IEEE Proceedings of the 12th International Conference on Wearable and Implantable Body Sensor Networks.
Komuro, N., Takaki, S., Suzuki, K., Citterio, D., 2013. Anal. Bioanal. Chem. 405 (17), 5785–5805.
Mattinen, U., Bobacka, J., Lewenstam, A., 2009. Electroanalysis 21 (17–18), 1955–1960.
Millan, M., Garcia-Granero, E., Flor, B., Garcia-Botello, S., Lledo, S., 2006. Dis. Colon Rectum 49 (5), 595–601.
Mir, M., Lugo, R., Tahirbegi, I.B., Samitier, J., 2014. Sensors 14 (7), 11844–11854.
Moschou, D., Trantidou, T., Regoutz, A., Carta, D., Morgan, H., Prodromakis, T., 2015. Sensors 15 (8), 18102–18113.
Nerstrom, M., Krarup, P.M., Jorgensen, L.N., Agren, M.S., 2016. World J. Gastrointest. Surg. 8 (5), 389–401.
Prodromakis, T., Liu, Y., Yang, J., Hollinghurst, D., Toumazou, C., 2011. IEEE Biomedical Circuits and Systems Conference, pp. 369–372.
Sjoberg, P., Maattanen, A., Vanamo, U., Novell, M., Ihalainen, P., Andrade, F.J., Bobacka, J., Peltonen, J., 2016. Sens. Actuators B-Chem. 224, 325–332.
Tahirbegi, I.B., Mir, M., Samitier, J., 2013. Biosens. Bioelectron. 40 (1), 323–328.
Tahirbegi, I.B., Mir, M., Schostek, S., Schurr, M., Samitier, J., 2014. Biosens. Bioelectron. 61, 124–130.
Trantidou, T., Payne, D.J., Tsiligkiridis, V., Chang, Y.C., Toumazou, C., Prodromakis, T., 2013. Sens. Actuators B-Chem. 186, 1–8.